

DOI: 10.1002/cmdc.201100510

Discovery of 2-(2-Benzoxazolyl amino)-4-Aryl-5-Cyanopyrimidine as Negative Allosteric Modulators (NAMs) of Metabotropic Glutamate Receptor 5 (mGlu₅): From an Artificial Neural Network Virtual Screen to an In Vivo Tool Compound

Ralf Mueller,^[a] Eric S. Dawson,^[b] Jens Meiler,^{*,[a]} Alice L. Rodriguez,^[b] Brian A. Chauder,^[b] Brittney S. Bates,^[b] Andrew S. Felts,^[b] Jeffrey P. Lamb,^[b] Usha N. Menon,^[b] Sataywan B. Jadhav,^[b] Alexander S. Kane,^[b] Carrie K. Jones,^[b, c] Karen J. Gregory,^[b, d] Colleen M. Niswender,^[b] P. Jeffrey Conn,^[b] Christopher M. Olsen,^[e] Danny G. Winder,^[e] Kyle A. Emmitte,^[a, b] and Craig W. Lindsley^{*,[a, b]}

Glutamate, the major excitatory neurotransmitter, functions in the brain via activation of ligand-gated cation channels and also the eight subtypes of class C G protein-coupled metabotropic glutamate receptors (mGlu_s).^[1] Selective allosteric modulation of mGlu₅ has been shown to have potential for treatment of a variety of neurological disorders,^[2,3] including anxiety disorders,^[4,5] Parkinson's disease,^[6-8] fragile X syndrome^[9] and schizophrenia.^[10-14] The majority of mGlu₅ negative allosteric modulators (NAMs) developed to date either contain an alkyne moiety, as in compounds 1–4, or employ the alkyne topology as basis for ligand design,^[15] as in compounds 5–8 (Figure 1). Only recently have mGlu₅ NAM chemotypes been identified, through high-throughput screening (HTS) campaigns, that are structurally unrelated to the classical acetylenic derivatives, such as compounds 9–12 (Figure 1).^[16] Due to the prevalence of a "molecular switch" phenomenon in 2-methyl-6-(phenylethynyl)pyridine (MPEP)-related scaffolds, our interest focused on the discovery and development of novel mGlu₅

NAM chemotypes, by both HTS and artificial neural network (ANN) virtual screens.

High-throughput screens leverage the often diverse chemical content found in collections of small molecules (10⁵–10⁶ compounds) to rapidly identify a subset of molecules with the desired activity via automated plate-based experimental assays.^[17] A recent PubChem search^[18] returned 120 HTS assays targeting G protein-coupled receptor (GPCR) signaling that addressed targets like RGS16-G_{αo} (AID1441, a primary screen reporting 826 active compounds out of 218,535 tested), and 5-hydroxytryptamine (serotonin) receptor subtype 1a (5-HT_{1A}) (AID567, a primary screen reporting 366 actives out of 64,907 compounds tested). The hit rates (0.4–0.6% active) in these examples are typical of HTS and highlight the frequently encountered limitation that approximately 99.5% of the screened compounds are routinely reported as inactive towards the desired screening target.^[18,19] Theoretically, the increase of this sparse hit rate by an order of magnitude (5% actives) would enrich the screening results and require that only 10% of the original total amount of compounds would need to be tested in a second round to roughly double the amount of active compounds identified. A systematic method capable of producing this level of enrichment by utilizing virtual screens would significantly reduce iterative screening costs and accelerate experimental turnaround times to facilitate more rapid discovery of novel leads.

Rodriguez and co-workers recently screened approximately 160 000 small molecules to identify allosteric modulators of mGlu₅ receptor signaling.^[19] The primary assay revealed 624 potential antagonists by reduction of calcium flux at an 80% maximally effective concentration of glutamate (EC₈₀) in an experimental screening protocol designed to detect various types of mGlu₅ allosteric modulation. In confirmatory screens that employed ten-point concentration–response curves, 345 mGlu₅ antagonists were verified.^[19] This experimental HTS data set formed the basis of model development for a virtual screen of the ChemDiv screening collection of over 700 000 compounds.^[20] Results of that virtual screen and pharmacological characterization of a selected set of the predicted compounds are described herein. Medicinal chemistry optimization of a new chemotype and characterization of a novel tool compound is also described, including assessment of in vivo efficacy in two different behavioral assays.

[a] Dr. R. Mueller, Prof. J. Meiler, Prof. K. A. Emmitte, Prof. C. W. Lindsley
Department of Chemistry, Vanderbilt University
7330 Stevenson Center, Station B 351822, Nashville, TN 37232-6600 (USA)
E-mail: jens.meiler@vanderbilt.edu
craig.lindsley@vanderbilt.edu

[b] Dr. E. S. Dawson, Dr. A. L. Rodriguez, Dr. B. A. Chauder, B. S. Bates,
Dr. A. S. Felts, J. P. Lamb, U. N. Menon, Dr. S. B. Jadhav, Dr. A. S. Kane,
Prof. Dr. C. K. Jones, Dr. K. J. Gregory, Prof. C. M. Niswender, Prof. P. J. Conn,
Prof. K. A. Emmitte, Prof. C. W. Lindsley
Vanderbilt Center for Neuroscience Drug Discovery
Department of Pharmacology
Vanderbilt University Medical Center (12475 MRBIV)
2213 Garland Avenue, Nashville, TN 37232-6600 (USA)

[c] Prof. Dr. C. K. Jones
U.S. Department of Veterans Affairs
Tennessee Valley Healthcare System (TVHS)
1310 24th Avenue South, Nashville, TN 37212 (USA)

[d] Dr. K. J. Gregory
Drug Discovery Biology
Monash Institute of Pharmaceutical Sciences, Monash University
Parkville, Victoria, 3052 (Australia)

[e] Dr. C. M. Olsen, Prof. D. G. Winder
Department of Molecular Physiology and Biophysics
Vanderbilt University Medical Center
1211 Medical Center Drive, Nashville, TN 37232-6600 (USA)

Supporting information for this article is available on the WWW under <http://dx.doi.org/10.1002/cmdc.201100510>.

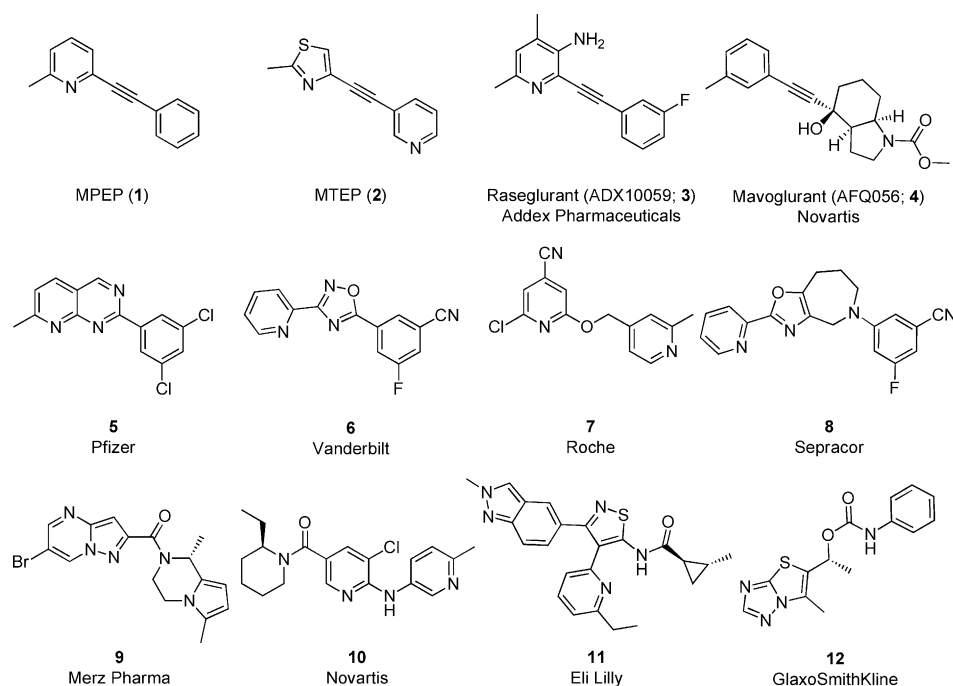


Figure 1. mGlu₅ NAM chemotypes represented by alkyne chemotypes 1–4, chemotypes based on the alkyne topology 5–8 and novel chemotypes not based on an acetylenic, MPEP-like scaffold or topology 9–12.

Structure–activity relationships (SARs) are built on the paradigm that structurally similar compounds typically have similar biological activity. Quantitative structure–activity relationships (QSARs) connect activity to structure by fitting a mathematical function through known SAR data: $f(\text{structure}) = \text{activity}$.^[21] Linear regression analysis is commonly used to establish QSAR models. However, this approach assumes that the biological activity can be described as a linear combination of all the structural descriptors, which is not necessarily the case. Machine learning tools like ANNs can alleviate this problem, since they employ nonlinear functions to relate input (structure) and output (activity), as described by Winkler and co-workers.^[22] The QSAR models reported here are neural networks employing one hidden layer with a variable number of inputs and hidden neurons trained with simple back-propagation of errors, or resilient propagation.^[23]

Once this quantitative relationship is established in a model, it can be employed to predict the activity of molecules with known structure but unknown activity. Our approach for establishing QSARs from HTS experiments includes four steps: 1) a dataset connecting molecules with known SAR needs to be obtained; 2) the structures of the molecules are described in a way that remains independent from spatial orientation (to avoid the need to perform lengthy superimpositions of the molecules); 3) training of models (ANNs) through supervised back-propagation of errors is performed; and 4) final prediction of molecular bioactivity at a given target without prior knowledge of activity for the query compounds is returned. Predicted active molecules from commercially available databases^[20] (e.g., ChemDiv, ChemBridge, Enamine) are then ordered and tested to validate the model's ability to enrich for compounds

with mGlu₅ pharmacologic activity. Noeske and co-workers^[24,25] recently utilized virtual screens that employed a machine learning self-organizing map (SOM) approach to search for mGlu₁ NAMs, and their efforts yielded one molecule showing potency below 1 μM , and five compounds with activities between 1 μM and 15 μM in a rat mGlu₁ experimental assay. We also have recently applied an initial version of ANN-based virtual HTS to identify new mGlu₅ positive allosteric modulators (PAMs).^[26]

Six models with different subsets of ADRIANA descriptors (Table 1) were trained.^[26–28] The ANN model trained on all 35 descriptor categories available in the ADRIANA^[29] descriptor set achieved a root mean square deviation (RMSD) value of 0.209, area under the curve (AUC)

value of 0.83, and a theoretical enrichment value of 18.8 for the independent data set. The descriptor subsets and model quality measures for AUC, RMSD, and enrichment are shown in Table 2. For the first round of model optimization, the four least sensitive descriptor categories were removed leading to an RMSD value of 0.199, an AUC value of 0.87, and an enrichment value of 28.2. Removal of eight more descriptor categories led to the optimal model with 763 descriptors and to an RMSD value of 0.201, an AUC value of 0.86, and a theoretical enrichment value of 37.6. Further reduction of the number of descriptors led to slightly inferior models that were not considered for further predictions (Figure 2). While the RMSD and AUC values represent the general quality of the trained ANNs, these metrics mainly capture the overall utility of the models to sort potentially active from likely inactive compounds. However, the success of a model is based primarily on the experimental enrichment of active compounds (true positives) for commercial orders and experimental testing. Therefore, the theoretical enrichment measure (see Supporting Information) was weighted more heavily in our final assessment of model metrics based on its closer correlation with the final experimental ratio of correctly identified compounds with mGlu₅ activity.

The ANN model with the highest theoretical enrichment for mGlu₅ NAMs was employed to virtually screen the ChemDiv Discovery Chemistry database of 708416 commercially available druglike compounds.^[20] At a 10 μM potency cutoff, the model predicted a set of 42041 active small molecules. Molecules with a weight above 600 Da, topological polar surface area greater than 130 \AA^2 , a calculated XlogP^[30] value greater than 4.0, or compounds that contained labile or reactive frag-

Table 1. Summary of 1252 molecular descriptors in 35 categories computed with ADRIANA.				
Type	Description method	Description property	Abbreviation	Number
1	Scalar	MW of compound	Weight	1
2	descriptors	No. H-Bond donors	HDon	1
3		No. H-Bond acceptors	HAcc	1
4		Oct/water part. coeff-ic.	XlogP	1
5		Polar surface area	TPSA	1
6		Molecular polariz.	Polariz	1
7		Dipole moment	Dipol	1
8		Solubility (water)	LogS	1
9	2D	Atom identities	2DA Ident	11
10	auto-	s atom charges	2DA SigChg	11
11	correlation	p atom charges	2DA PiChg	11
12		Total charges	2DA TotChg	11
13		s atom electroneg.	2DA SigEN	11
14		p atom electroneg.	2DA PiEN	11
15		Lone pair electroneg.	2DA LpEN	11
16		Effective atom polariz.	2DA Polariz	11
17	3D	Atom identities	3DA Ident	12
18	auto-	s atom charges	3DA SigChg	12
19	correlation	p atom charges	3DA PiChg	12
20		Total charges	3DA TotChg	12
21		s atom electroneg.	3DA SigEN	12
22		p atom electroneg.	3DA PiEN	12
23		Lone pair electroneg.	3DA LpEN	12
24		Effective atom polariz.	3DA Polariz	12
25	Radical	Atom identities	RDF Ident	128
26	distribution	s atom charges	RDF SigChg	128
27	function	p atom charges	RDF PiChg	128
28		Total charges	RDF TotChg	128
29		s atom electroneg.	RDF SigEN	128
30		p atom electroneg.	RDF PiEN	128
31		Lone pair electroneg.	RDF LpEN	128
32		Effective atom polariz.	RDF Polariz	128
33	Surface	Mol. Electrostat. pot.	Surf ESP	12
34	auto-	H-Bonding pot.	Surf HBP	12
35	correlation	Hydrophobicity pot.	Surf HPP	12
Total				1252

Table 2. The root mean square deviation (RMSD), area under the curve (AUC) and enrichment values for all mGlu ₅ NAMs QSAR models. ^[a]					
Descriptor Number	Type	Train	RMSD monitor ^[a]	AUC	Enrich. ^[b]
1252	1–35	0.184	0.203 (0.209)	0.83	18.8
972	1–19, 21–26, 29–32, 34–35	0.168	0.202 (0.199)	0.87	28.2
763	1–9, 11, 12, 14, 15, 17, 21–23, 25, 29–32, 35	0.157	0.201 (0.201)	0.86	37.6
683	1–8, 14, 23, 25, 29–32, 35	0.178	0.204 (0.210)	0.84	9.4
555	1–8, 14, 23, 25, 29–31, 35		0.204 (0.218)	0.81	28.2
416	1–8, 23, 25, 30, 31, 35		0.210 (0.215)	0.82	9.4

[a] Number in parentheses is the independent value. [b] Enrichment (enrich.) determined at 0.3%.

ments were removed via automated filtration.^[31,32] Further removal of molecules with a Tanimoto substructure^[33] similarity value above 0.6 reduced the predicted active compounds to

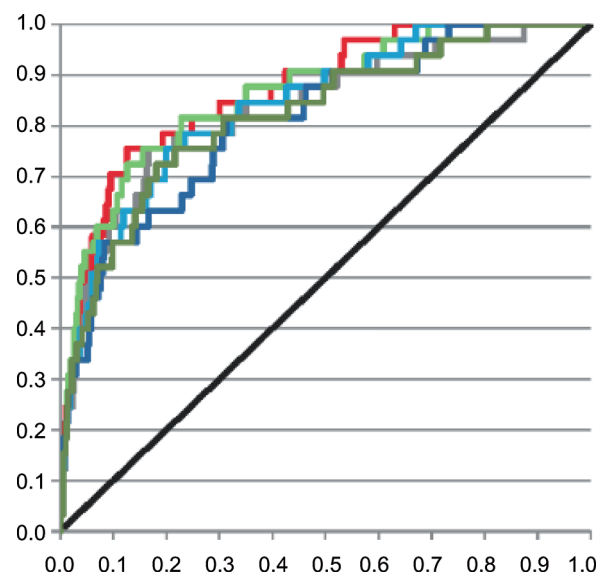


Figure 2. Receiver operating characteristic (ROC) curve plot for models using base (—), 416 (—), 555 (—), 683 (—), 763 (—), 972 (—), and 1252 (—) descriptors. While the models with 972 (—) and 763 (—) descriptors performed well over the entire ROC curve, the other models clearly show a reduced performance in the middle portion. The steepness at the beginning of the curve most effects theoretical enrichment, however, all of the models displayed similar performance for total area under the curve (AUC). Therefore, based on significantly better theoretical enrichment values, the model with 763 descriptors (—) was selected for final prediction of active compounds to be ordered.

be ordered to 749. These compounds were tested at the Vanderbilt Institute for Chemical Biology High-Throughput Screening Center^[34] to reveal a single-point concentration (change in signal amplitude of at least three standard deviations from vehicle) experimental hit rate of 12% (88/749 compounds) that included a putative 51 NAMs, 18 PAMs and 19 agonists. Concentration–response curves (CRCs) formed of ten data points ranging from 1 nM to 30 μ M confirmed the identification of 12 NAMs, 14 PAMs and one partial agonist ($EC_{50}/IC_{50} < 30 \mu$ M; 3.6% overall hit rate) representing an enrichment factor of 15.7 for mGlu₅ activity compared with the original mGlu₅ experimental HTS data (0.22% original experimental hit rate). Compounds with confirmed antagonist activity (1.6% of predicted compounds) were enriched by a factor of 7.0 with novel mGlu₅ NAM scaffolds. The optimized mGlu₅ ANN models recognized substructure patterns related nonlinearly to biological activity in chemical scaffolds that were not used in training the method and thus allowed for identification of previously unknown mGlu₅ NAMs with novel chemotypes (Figure 3).^[35] The discovery of two novel, potent mGlu₅ NAMs **13** and **14**, with IC_{50} values of 75 and 124 nM, respectively, possessing a previously unknown scaffold demonstrates the success of this approach.

Particularly interesting among the confirmed active compounds from the ANN virtual screen were the two potent 2-(2-benzoxazolylamino)-4-phenylpyrimidines **13** and **14**, differing only in the substituent at the 5-position of the pyrimidine ring. Structurally, these compounds represent a significant departure from known mGlu₅ NAM chemotypes. Whereas analogue **13**

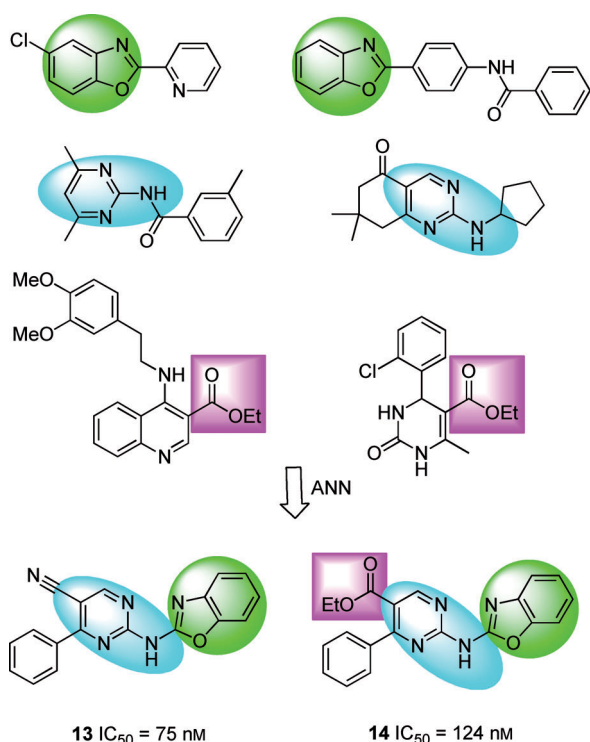


Figure 3. ANN pattern recognition of substructure fragments from known mGlu₅ NAMs identified novel combinations of substructures with potent mGlu₅ NAM activity. Highlighted substructures exist in several compounds in the training set from separate scaffolds. The optimized mGlu₅ ANN model identified potent mGlu₅ NAMs **13** and **14** that combined two or more of these features into the same scaffold.

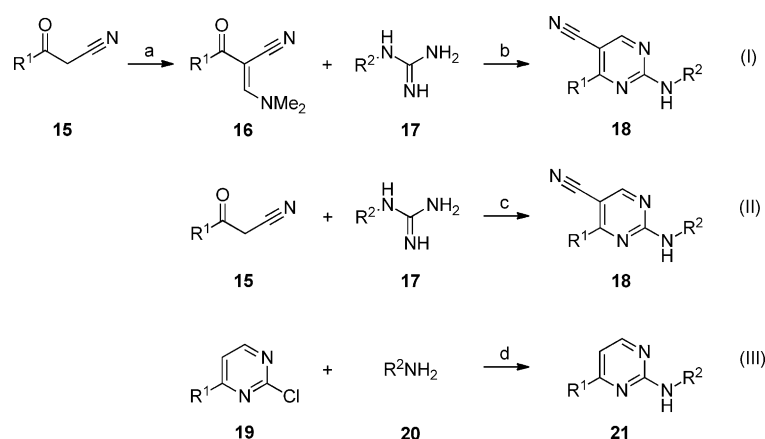
contained a 5-cyano group, the corresponding group on compound **14** was an ethyl ester. Although esters are generally not suitable for use in many applications due to esterase-mediated metabolism, cyano groups are often tolerated. The scaffold was quite attractive for a medicinal chemistry optimization program as there were multiple portions of the molecule amenable to modification and SAR development. Efforts were thus focused toward that objective.

Synthetic routes used to prepare the target compounds were quite straightforward (Scheme 1). In order to access the 5-cyanopyrimidine targets with the generic structure **18**, two different routes that both began with β -ketonitriles **15** were employed. Many β -ketonitriles are commercially available or can easily be prepared through additions of cyanomethanide anion to simple alkyl esters.^[36] In part (I) of Scheme 1, **15** was treated with *N,N*-dimethylformamide/dimethyl acetal (DMF/DMA) to afford intermediate **16**, which was subsequently reacted with substituted guanidines **17** under basic conditions to afford **18**. Alternatively, as shown in part (II) of Scheme 1, **15** could be reacted directly with **17** in the presence of triethyl orthoformate to produce **18**, and this approach was generally preferred due to superior yields and fewer side reactions. For analogues lacking a 5-cyano substituent such as **21**, palladium-mediated coupling of amines **20** with 2-chloropyridine **19** were

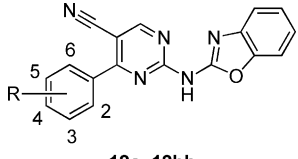
employed (part (III) of Scheme 1). Using the synthetic routes described allowed for evaluation of three distinct areas of the chemotype: the necessity of the 5-cyano substituent, the SAR at the 6-position of the pyrimidine ring (R^1), and the SAR around the 2-amino substituent (R^2).

Initial SAR exploration focused on substitution at the 4- and 5-positions of the pyrimidine core, as well as on the 2- and 3-positions of the phenyl ring. The resynthesis of hit compound **13** gave potency in good agreement with that observed with the original batch (IC_{50} = 89 nM). Removal of the 5-cyano substituent resulted in a dramatic loss of potency (IC_{50} > 10 μ M), as did the introduction of a 4-methyl substituent on the pyrimidine ring (IC_{50} > 30 μ M). Isosteric replacements for the 2-amino benzoxazole, such as benzothiazoles, benzimidazoles, quinolines and pyridines, also gave compounds with diminished potency at mGlu₅ (IC_{50} > 30 μ M). In light of such data, the decision was made to focus SAR development on analogues containing the key 5-cyano substituent on the pyrimidine core and the 2-amino benzoxazole moiety at R^2 .

Further development of SAR around substitution of the phenyl ring was continued in the context of the 5-cyanopyrimidine core (Table 3). In order to evaluate the effect of substituents of varying electronic character, methyl, chloro, and methoxy analogues were prepared at each position (**18a–i**). Both the 2-methoxyphenyl analogue (**18g**) and the 4-methylphenyl analogue (**18c**) had similar activities to hit compound **13**. Other analogues demonstrated reduced potency relative to **13** with 3-chlorophenyl **18e** being considerably less potent. Fluorophenyl analogues were more active than their chlorophenyl comparators (compare **18j** with **18d** and **18k** with **18f**), and analogue **18k** was equipotent to **13**. Several analogues with larger electron-withdrawing groups were either inactive or weak antagonists (**18l–p**). The size of the substituent on the phenyl ring was key to potency as evidenced by 4-ethylphenyl analogue **18q** (compare with **18c**) and 2-ethoxyphenyl analogue **18r** (compare with **18g**). A number of disubstituted analogues were prepared (**18s–18bb**), and these compounds were generally weak antagonists. The exceptions were 4-chloro-2-fluorophenyl analogue **18y**, 4-fluoro-2-methoxy-



Scheme 1. Reagents and conditions: a) $Me_2NCH(OMe)_2$, DMF; b) CS_2CO_3 , DMF, μ w, 200 °C, 10 min (5–40% over two steps); c) $HC(OEt)_3$, 140 °C (50–75%); d) $Pd_2(dba)_3$, CS_2CO_3 , xantphos, dioxane, μ w, 140 °C, 20 min (10–50%).

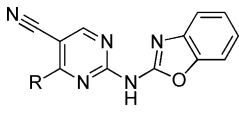
Table 3. Structures and activities of 5-cyanopyrimidine analogues **18**.


Compd	R	IC ₅₀ [nM] ^[a]	% Glu Max ^[b]
13	H	89 ± 32	1.9 ± 3
18 a	2-CH ₃	403 ± 47	1.9 ± 0.4
18 b	3-CH ₃	138 ± 47	3.6 ± 1.1
18 c	4-CH ₃	90 ± 32	2.6 ± 0.7
18 d	2-Cl	516 ± 54	2.2 ± 0.5
18 e	3-Cl	2830 ± 1320	3.2 ± 0.8
18 f	4-Cl	315 ± 110	2.5 ± 0.5
18 g	2-OCH ₃	62 ± 10	0.9 ± 0.4
18 h	3-OCH ₃	266 ± 47	2.4 ± 0.3
18 i	4-OCH ₃	223 ± 74	2.1 ± 0.3
18 j	2-F	258 ± 51	1.8 ± 0.4
18 k	4-F	91 ± 22	1.7 ± 0.1
18 l	3-CF ₃	> 30000	–
18 m	4-CF ₃	> 30000	–
18 n	3-Br	> 30000	–
18 o	4-Br	4120 ± 1860	3.8 ± 1.2
18 p	4-OCF ₃	> 30000	–
18 q	4-CH ₂ CH ₃	1530 ± 358	2.8 ± 0.5
18 r	2-OCH ₂ CH ₃	6580 ± 1670	4.5 ± 0.9
18 s	2,3-di-F	1910 ± 773	2.5 ± 0.3
18 t	3,4-di-F	2580 ± 1170	9.6 ± 0.7
18 u	2,4-di-Cl	666 ± 238	3.0 ± 0.4
18 v	3,4-di-Cl	> 10000 ^[c]	46 ± 13
18 w	3,5-di-Cl	> 30000	–
18 x	3,5-di-OCH ₃	> 10000 ^[c]	24 ± 10
18 y	2-F, 4-Cl	375 ± 90	1.8 ± 0.5
18 z	2-OCH ₃ , 4-F	217 ± 10	1.5 ± 0.4
18 aa	2-OCH ₃ , 4-Cl	148 ± 42	2.0 ± 0.2
18 bb	3-F, 4-OCH ₃	1060 ± 696	2.9 ± 0.6

[a] IC₅₀ values are the average of at least three determinations. [b] % Glu Max is the maximum response of compounds relative to the maximal glutamate response. Data are the mean of at least three determinations. [c] CRC does not plateau.^[35]

phenyl analogue **18z**, and 4-chloro-2-methoxyphenyl analogue **18aa**, which were only slightly less potent than **13**. Interestingly, analogue **18z** was less potent than both **18g** and **18k**, which was somewhat surprising.

Having identified several similarly potent mGlu₅ NAMs in this manner, subsequent efforts focused on the replacement of the phenyl ring (R¹) altogether. A variety of 5- and 6-membered heterocycles were evaluated with limited benefit (Table 4). The evaluation of pyridine (**18cc** and **18dd**) and thiophene (**18ee** and **18ff**) isosteres revealed that these were not well tolerated, although 3-pyridyl analogue **18dd** remained moderately potent. Similarly, naphthyl analogues such as **18gg** and **18hh** were only weak antagonists. Finally, introduction of a cyclohexyl group (**18ii**) resulted in only an approximately threefold decrease in potency relative to **13**. The tolerance for the cyclohexyl ring is a bit surprising given the sensitivity demonstrated with other analogues (such as **18ee** and **18ff**) that are much more similar in size to hit compound **13**. Based on the SARs elucidated from the analogues presented thus far, it was deter-

Table 4. Structures and activities of further 5-cyanopyrimidine analogues **18**.


Compd	R	IC ₅₀ [nM] ^[a]	% Glu Max ^[b]
18 cc	pyridin-2-yl	> 10000 ^[c]	22 ± 2
18 dd	pyridin-3-yl	500 ± 23	2.1 ± 0.7
18 ee	thiophen-2-yl	> 10000 ^[c]	35 ± 10
18 ff	thiophen-3-yl	4740 ± 1530	13 ± 5
18 gg	naphthalen-2-yl	> 10000 ^[c]	47 ± 11
18 hh	naphthalen-1-yl	> 10000 ^[c]	40 ± 12
18 ii	cyclohexyl	216 ± 71	3.8 ± 0.8

[a] IC₅₀ values are the average of at least three determinations. [b] % Glu Max is the maximum response of compounds relative to the maximal glutamate response. Data are the mean of at least three determinations. [c] CRC does not plateau.^[35]

mined that potency was substantially influenced by relatively minor changes in this portion of the chemotype. Such observations are quite common with mGlu₅ NAMs from other chemotypes and have been noted in the literature.^[37–40] A final effort was made to introduce substituents onto various positions of the benzoxazole ring; however, even small groups such as methyl and fluoro were not generally tolerated.

Having a number of compounds with good functional potency in hand, an evaluation of the metabolic stability of several compounds was in order. Compounds of interest were examined with regard to their stability in human and mouse liver microsomes following 15 min of incubation.^[41] A general trend of greater stability in human compared to mouse liver microsomes was noted. Enhanced stability relative to **13** was observed with 4-substituted phenyl analogues **18c**, **18i**, and **18k**.^[35] The nature of the 4-substituent does not appear to be a determining factor as these compounds have similar stabilities in both species. Although there was little difference between their respective metabolic profiles in microsomes, the methyl group of **18c** was still viewed as a risk for in vivo oxidative metabolism. The fluorophenyl analogue **18k** offered a convenient and equipotent alternative without such a concern.

Consideration of the SAR and the stability data in mouse liver microsomes indicated that compound **18k** would be a potentially interesting compound for evaluation in an in vivo pharmacokinetics study. Prior to initiation of that study, more detailed molecular pharmacology studies with **18k** were conducted. A radioligand binding study (Figure 4b) measuring the ability of the compound to compete with the equilibrium of [³H]-3-methoxy-5-(pyridin-2-ylethynyl)pyridine (MeOPEPy),^[42] a close structural analogue of MPEP (**1**), confirmed the interaction of **18k** with the known mGlu₅ allosteric binding site (mGlu₅ K_i = 84 ± 14 nM). We evaluated the effects of **18k** in a native system, rat cortical astrocytes, where mGlu₅-mediated responses have previously been studied.^[43,44] Compound **18k** induced a rightward shift in the glutamate CRC and reduced the maximal effect of glutamate (Figure 4c), confirming activity

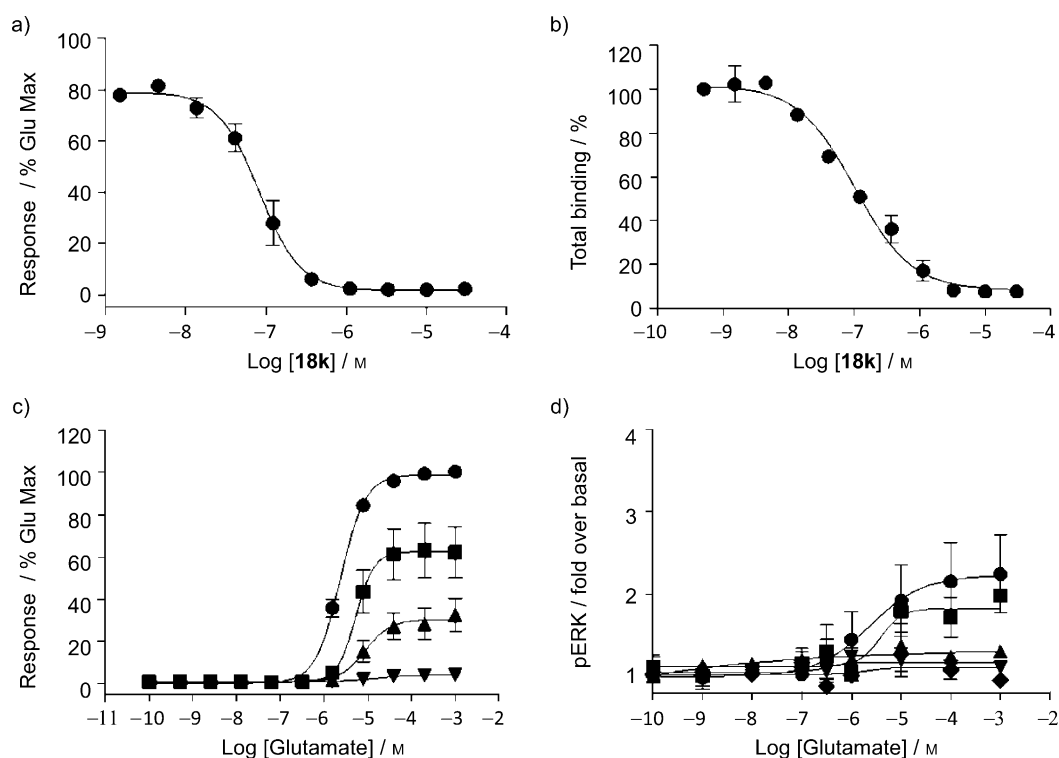


Figure 4. In vitro characterization of **18k**. a) Concentration–response curve (CRC) derived from an mGlu₅ calcium mobilization assay ($IC_{50} = 91 \pm 22$ nM, % Glu Max = 1.7 ± 0.1 %); b) Competition binding CRC between **18k** and [³H]MeOPEPY affording a K_i value of 84 ± 14 nM, suggesting **18k** is fully competitive with the classical MPEP allosteric site in mGlu₅; c) Effect of **18k** on glutamate CRC in rat cortical astrocytes (● = glutamate + vehicle; ■ = glutamate + 300 nM **18k**; ▲ = glutamate + 1 μM **18k**; ▼ = glutamate + 30 μM **18k**); d) Effect of **18k** on glutamate-induced ERK phosphorylation in mGlu₅-expressing HEK293 cells (● = glutamate + vehicle; ■ = glutamate + 10 nM **18k**; ▲ = glutamate + 30 nM **18k**; ▼ = glutamate + 100 nM **18k**; ◆ = glutamate + 1 μM **18k**). Data represent the mean \pm standard error of the mean (SEM) of at least three independent experiments.

in the native system and suggesting noncompetitive inhibition of the glutamate response.

It was also important to examine the effects of **18k** in multiple signaling pathways, as it has been shown that mGlu₅ allosteric modulators can have an effect through some pathways and not others.^[43,44] To this end, we determined the effects of **18k** on the ERK1/2 phosphorylation response to glutamate in HEK293 cells expressing rat mGlu₅. We found **18k** blocked the effect of glutamate in a concentration-dependent manner (Figure 4d), confirming antagonist activity in the ERK pathway. Examination of the activity of compound **18k** against other mGlu receptors^[35] revealed no observable activity at 10 μM against mGlu₁₋₄ and mGlu₆₋₈. Compound **18k** was also run at 10 μM in Ricerca Bioscience's LeadProfilingScreen,^[45] which evaluates the test compound in radioligand binding assays for 68 primary molecular targets from classes such as GPCRs, kinases, and ion channels, including many targets relevant to central nervous system (CNS) drug discovery. In this screen, an inhibition of more than 50% of radioligand binding was observed only in the adenosine A₃ receptor assay (73% inhibition of binding), indicating that **18k** has a remarkably clean pharmacology profile.

Confident of the molecular pharmacology profile, a study of the exposure of **18k** following oral (p.o.) dosing in mice was conducted.^[35] Unfortunately, the results revealed no exposure above detectable limits in either plasma or brain. As such, the

compound was subsequently studied using intraperitoneal (i.p.) dosing (Table 5). Although exposure of **18k** was only moderate in plasma ($AUC = 224$ ng h mL⁻¹), the brain exposure was quite good ($AUC = 1006$ ng h g⁻¹) giving a brain to plasma ratio of 4:1.^[46] Protein binding studies revealed that compound

Table 5. Plasma and brain exposure of **18k** in mice.

Time [h]	Concentration [ng mL ⁻¹]		Brain:Plasma ratio
	Plasma (■)	Brain (▲)	
0.5	31.8	136	4.3
1	64.7	283	4.4
3	45.4	193	4.3
6	9.2	68	7.4

All animal work was performed in accordance with Vanderbilt Institutional Animal Care and Use Committee (IACUC) policies and approved procedures for the ethical use and treatment of animals.

18k is highly bound in both mouse plasma (99.4%) and mouse brain homogenates (99.5%).^[47] While limited free fraction represented a concern for the ability of **18k** to function in an in vivo behavior study, the brain exposure data argued for its evaluation in spite of this fact.

Ideally, evaluation of a new tool compound such as **18k** in a behavioral assay would initially take place in an assay known to be sensitive to other mGlu₅ antagonists. It has been established that mice will bury foreign objects such as glass marbles in deep bedding.^[48] Furthermore, studies have shown that low doses of anxiolytic benzodiazepines inhibit this behavior.^[49] Additionally, the well known mGlu₅ NAM tool compounds MPEP (**1**) and fenobam are effective in this model.^[50–52] Marble burying is also an operationally convenient assay, making it useful in an in vivo screening paradigm. We examined compound **18k** as well as MTEP (positive control) in this assay using a 15 min pretreatment with both compounds (Figure 5). Robust inhibition of marble burying with the 15 mg kg⁻¹ dose of MTEP was observed as expected. Significant inhibition of marble

burying was also observed with **18k** at the highest dose of 56.6 mg kg⁻¹. Consideration of the results in the context of the pharmacokinetic study provided some insight. In mice, the average brain concentration of **18k** at 30 min was 0.41 μM, while the brain concentration at 1 h post-treatment was 0.85 μM. The marble burying assay was conducted between the 15 and 45 min time points post-dose, so the brain concentrations at these time points are relevant. If a dose linear increase in exposure is assumed, a 56.6 mg kg⁻¹ dose should lead to brain exposures between 2.3 and 4.8 μM. It is certainly possible that the highly protein bound nature of **18k** is restricting the availability of free drug to interact with the receptor, thus necessitating relatively high brain concentrations in order to achieve efficacy.

Seeking to examine compound **18k** in a behavioral model of addiction, focus turned to a relatively new model. C57Bl/6J mice readily acquired operant responding to varied visual and auditory stimuli without prior training, a phenomenon termed operant sensation seeking (OSS).^[53,54] During this assay, mice will “self-administer” visual cues consisting of flashing lights of random duration in combination with an auditory stimulus. Recent studies using low doses of the dopamine antagonist *cis*-flupenthixol to disrupt dopamine signaling demonstrated increased responding for OSS stimuli, similar to effects seen with cocaine self-administration.^[55] Furthermore, mice lacking mGlu₅ also fail to acquire OSS despite having normal acquisition of food self-administration,^[56] suggesting that OSS would represent another interesting assay for assessment of novel mGlu₅ NAMs with therapeutic potential for addiction. Since it has also been established that mGlu₅ knockout mice do not self-administer cocaine,^[57] the reinforcing effects of OSS may in fact be more similar to psychostimulants than food. Recently, the results of studies with both MTEP and the first novel small-molecule mGlu₅ NAM were reported in the OSS model.^[58] Gratifyingly, compound **18k** also dose dependently reduced progressive ratio responding for OSS stimuli with no significant effects observed with a food reinforcer (Figure 6).^[53,54,56,58] Unlike the marble burying assay, here significant effi-

cacy was observed at both the 30 and 56.6 mg kg⁻¹ doses of **18k**.

In summary, we have developed a novel mGlu₅ NAM tool compound from a completely new 4-aryl-5-cyanopyrimidine chemotype, identified through an ANN virtual screening exercise. Although SAR in this series was somewhat flat, some compounds with excellent potency were identified. Compound **18k** is a potent noncompetitive antagonist in vitro that interacts with the known allosteric bind-

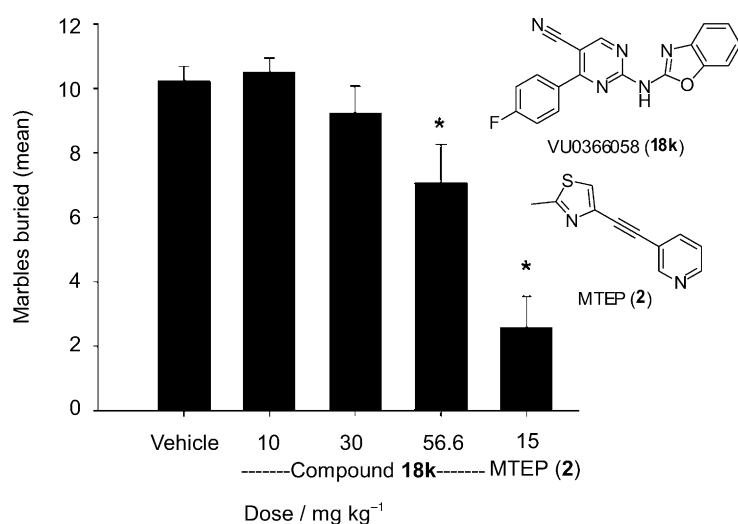


Figure 5. In vivo characterization of **18k**. Inhibition of marble burying with **18k** (VU0366058) relative to MTEP (**2**). Dosing (i.p.) vehicle was 10% tween 80. No sedation was observed in any groups ($n = 12$ per dosing group). Significance was determined as $p < 0.05$ versus vehicle control group (Dunnett's test).

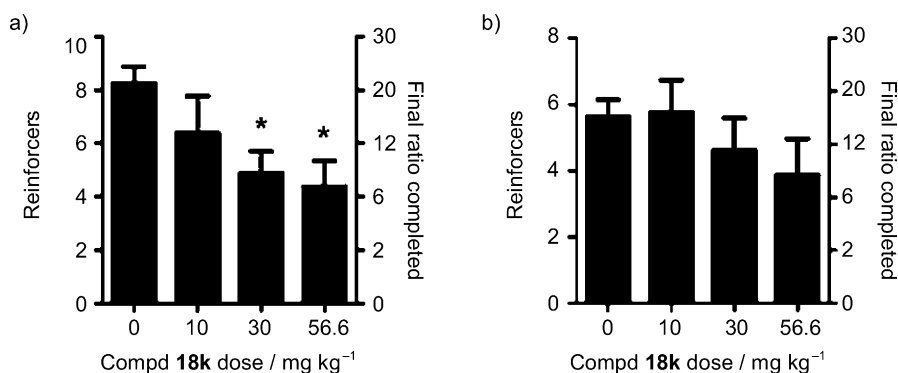


Figure 6. Efficacy of compound **18k** in the operant sensation seeking (OSS) model of addiction: a) OSS ($n = 8$); b) food ($n = 6$). Dosing (i.p.) vehicle was 10% tween 80. Significance was determined as $p < 0.05$ versus vehicle control group (Dunnett's test).

ing site. It is also selective for mGlu₃ over other mGlu receptors and demonstrated excellent selectivity in a large, diverse panel of other drug targets. When examined in the marble burying model of anxiety and the OSS model of addiction, compound **18k** demonstrated efficacy. Although the molecule lacks oral bioavailability in mice and is highly protein bound, these features are overcome by intraperitoneal (i.p.) dosing and the excellent brain to plasma ratio exhibited by compound **18k**. Of particular value is the demonstration that the ANN screening approach employed here can be used as a viable method for the identification of fundamentally new chemotypes. Further studies including additional in vivo profiling of compound **18k** are planned and will be reported in due course.

Acknowledgements

The authors warmly thank the US National Institutes of Health (NIH), and in particular the US National Institute on Drug Abuse (NIDA; R01DA023947-01) and the US National Institute of Mental Health (NIMH; R01090192-01), for support of our programs in drug discovery. The authors also thank Daryl F. Venable (Vanderbilt University, Nashville, USA) for technical assistance with the calcium flux and radioligand binding assays.

Keywords: addiction · allosteric modulators · artificial neural networks · metabotropic glutamate receptors · structure-activity relationships

- [1] C. M. Niswender, P. J. Conn, *Annu. Rev. Pharmacol. Toxicol.* **2010**, *50*, 295–322.
- [2] F. Gasparini, G. Bilbe, B. Gomez-Mancilla, W. Spooren, *Curr. Opin. Drug Discovery Dev.* **2008**, *11*, 655–665.
- [3] P. J. Conn, A. Christopoulos, C. W. Lindsley, *Nat. Rev. Drug Discovery* **2009**, *8*, 41–54.
- [4] R. H. Porter, G. Jaeschke, W. Spooren, T. M. Ballard, B. Buttelmann, S. Kolczewski, J.-U. Peters, E. Prinssen, J. Wichmann, E. Viera, A. Muhlemann, S. Gatti, V. Mutel, P. Malherbe, *J. Pharmacol. Exp. Ther.* **2005**, *315*, 711–721.
- [5] C. J. Swanson, M. Bures, M. P. Johnson, A. M. Linden, J. A. Monn, D. D. Schoepp, *Nat. Rev. Drug Discovery* **2005**, *4*, 131–144.
- [6] M. J. Marino, P. J. Conn, *Curr. Drug Targets: CNS Neurol. Disord.* **2002**, *1*, 239–250.
- [7] M. J. Marino, H. Awad, O. Poisik, M. Wittmann, P. J. Conn, *Amino Acids* **2002**, *23*, 185–191.
- [8] M. Marino, O. Valenti, P. J. Conn, *Drugs Aging* **2003**, *20*, 377–397.
- [9] M. F. Bear, K. M. Huber, S. T. Warren, *Trends Neurosci.* **2004**, *27*, 370–377.
- [10] M. J. Marino, P. J. Conn, *Curr. Drug Targets: CNS Neurol. Disord.* **2002**, *1*, 1–16.
- [11] B. Moghaddam, *Psychopharmacology* **2004**, *174*, 39–44.
- [12] G. G. Kinney, M. Burno, U. C. Campbell, L. M. Hernandez, D. Rodriguez, L. J. Bristow, P. J. Conn, *J. Pharmacol. Exper. Ther.* **2003**, *306*, 116–123.
- [13] P. J. Conn, C. W. Lindsley, C. K. Jones, *Trends Pharmacol. Sci.* **2009**, *30*, 25–31.
- [14] C. M. Niswender, C. K. Jones, P. J. Conn, *Curr. Top Med. Chem.* **2005**, *5*, 847–857.
- [15] C. W. Lindsley, K. A. Emmitte, *Curr. Opin. Drug Discovery Dev.* **2009**, *12*, 446–457.
- [16] K. A. Emmitte, *ACS Chem. Neurosci.* **2011**, *2*, 411–432.
- [17] K. H. Bleicher, H.-J. Böhm, K. Müller, A. I. Alanine, *Nat. Rev. Drug Discovery* **2003**, *2*, 369–378.
- [18] The PubChem search was performed April 2011; <http://pubchem.ncbi.nlm.nih.gov/>.
- [19] A. L. Rodriguez, M. D. Grier, C. K. Jones, E. J. Herman, A. S. Kane, R. L. Smith, R. Williams, Y. Zhou, J. E. Marlo, E. L. Days, T. N. Blatt, S. Jadhav, U. Menon, P. N. Vinson, J. M. Rook, S. R. Stauffer, C. M. Niswender, C. W. Lindsley, C. D. Weaver, P. J. Conn, *Mol. Pharmacol.* **2010**, *78*, 1105–1123.
- [20] ChemDiv Inc. (San Diego, USA); <http://www.chemdiv.com/>.
- [21] C. Hansch, D. Hoekman, A. Leo, D. Weininger, C. D. Selassie, *Chem. Rev.* **2002**, *102*, 783–812.
- [22] D. Winkler, *Mol. Biotechnol.* **2004**, *27*, 139–167.
- [23] M. Riedmiller, H. Braun, *Proc. Int. Conf. Neural Networks* **1993**, 586–591.
- [24] T. Noeske, A. Jirgensons, I. Starchenkovs, S. Renner, I. Jaunzeme, D. Trifanova, M. Hechenberger, T. Bauer, V. Kauss, C. G. Parsons, G. Schneider, T. Weil, *ChemMedChem* **2007**, *2*, 1763–1773.
- [25] T. Noeske, D. Trifanova, V. Kauss, S. Renner, C. G. Parsons, G. Schneider, T. Weil, *Bioorg. Med. Chem.* **2009**, *17*, 5708–5715.
- [26] R. Mueller, A. L. Rodriguez, E. S. Dawson, M. Butkiewicz, S. Oleskiewicz, A. Bleckmann, C. D. Weaver, C. W. Lindsley, P. J. Conn, J. Meiler, *ACS Chem. Neurosci.* **2010**, *1*, 288–305.
- [27] J. Zupan, J. Gasteiger, *Neural Networks for Chemists—An Introduction*, VCH, Weinheim, **1993**.
- [28] J. Gasteiger, C. Rudolph, J. Sadowski, *Tetrahedron Computer Methodology* **1990**, *3*, 537–547.
- [29] C. H. Schwab, D. Hristozov, J. Gasteiger, ADRIANA.Code: Algorithms for the Encoding of Molecular Structures (version 2.0), Molecular Networks GmbH, Erlangen, Germany, **2006**; <http://www.molecular-networks.com/>.
- [30] R. Wang, Y. Gao, L. Lai, *Perspect. Drug Discovery Des.* **2000**, *19*, 47–66.
- [31] H. Bauknecht, A. Zell, H. Bayer, P. Levi, M. Wagener, J. Sadowski, J. Gasteiger, *J. Chem. Inf. Comput. Sci.* **1996**, *36*, 1205–1213.
- [32] J. Sadowski, M. Wagener, J. Gasteiger, *Angew. Chem.* **1995**, *107*, 2892–2895; *Angew. Chem. Int. Ed. Engl.* **1995**, *34*, 2674–2677.
- [33] A. R. Dominguez, A. K. Nandi, *Med. Phys.* **2007**, *34*, 4256–4269.
- [34] Vanderbilt Institute for Chemical Biology, High-throughput Screening Core (Nashville, USA); <http://www.vanderbilt.edu/hts/>.
- [35] For complete details, see the Experimental Section given in the Supporting Information.
- [36] Y. Ji, W. C. Trenkle, J. V. Vowels, *Org. Lett.* **2006**, *8*, 1161–1163.
- [37] A. S. Felts, S. R. Lindsley, J. P. Lamb, A. L. Rodriguez, U. N. Menon, S. Jadhav, C. K. Jones, P. J. Conn, C. W. Lindsley, K. A. Emmitte, *Bioorg. Med. Chem. Lett.* **2010**, *20*, 4390–4394.
- [38] S. Sharma, A. L. Rodriguez, P. J. Conn, C. W. Lindsley, *Bioorg. Med. Chem. Lett.* **2008**, *18*, 4098–4101.
- [39] A. L. Rodriguez, Y. Nong, N. K. Sekaran, D. Alagille, G. D. Tamagnan, P. J. Conn, *Mol. Pharmacol.* **2005**, *68*, 1793–1802.
- [40] M. R. Wood, C. R. Hopkins, J. T. Brogan, P. J. Conn, C. W. Lindsley, *Biochemistry* **2011**, *50*, 2403–2410.
- [41] The test compounds (1 μM) were incubated in medium containing human/mouse liver microsomes, phosphate buffer, and the cofactor NADPH, for 15 min at 37 °C with shaking.
- [42] N. D. P. Cosford, J. Roppe, L. Tehrani, E. J. Schweiger, T. J. Seiders, A. Chaudary, S. Rao, M. A. Varney, *Bioorg. Med. Chem. Lett.* **2003**, *13*, 351–354.
- [43] Y. Zhang, A. L. Rodriguez, P. J. Conn, *J. Pharmacol. Exp. Ther.* **2005**, *315*, 1212–1219.
- [44] M. J. Noetzel, J. M. Rook, P. N. Vinson, H. P. Cho, E. Days, Y. Zhou, A. L. Rodriguez, H. Lavreysen, S. R. Stauffer, C. M. Niswender, Z. Xiang, J. S. Daniels, C. W. Lindsley, C. D. Weaver, P. J. Conn, *Mol. Pharmacol.* **2011**, in press; DOI: 10.1124/mol.111.075184.
- [45] LeadProfilingScreen by Ricerca Bioscience, LLC (Concord, USA); <https://pharmacology.ricerca.com/catalog/>.
- [46] Compound **18k** was dosed at 10 mg kg⁻¹ (i.p.) as a microsuspension in 10% tween 80 in male CD-1 mice using two mice per time point. Brain and plasma samples were collected at 0.5, 1, 3, and 6 h post dose. Intraperitoneal (i.p.) dosing was chosen as a convenient route to help maximize exposure.
- [47] A 96-well rapid equilibrium dialysis (RED) apparatus (Thermo Scientific) was used to determine the free fraction of **25** in mouse plasma and brain homogenates.
- [48] R. M. J. Deacon, *Nat. Protoc.* **2006**, *1*, 122–124.
- [49] K. Njung'e, S. L. Handley, *Br. J. Pharmacol.* **1991**, *104*, 105–112.
- [50] C. L. Broekkamp, H. W. Rijk, D. Joly-Gelouin, K. L. Lloyd, *Eur. J. Pharmacol.* **1986**, *126*, 223–229.

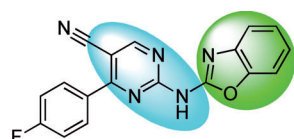
- [51] W. P. Spooren, A. Vassout, H. C. Neijt, R. Kuhn, F. Gasparini, S. Roux, R. D. Porsolt, C. Gentsch, *J. Pharmacol. Exp. Ther.* **2000**, *295*, 1267–1275.
- [52] L. B. Nicolas, Y. Kolb, E. P. M. Prinssen, *Eur. J. Pharmacol.* **2006**, *547*, 106–115.
- [53] C. M. Olsen, D. G. Winder, *Neuropsychopharmacology* **2009**, *34*, 1685–1694.
- [54] C. M. Olsen, D. G. Winder, *J. Visualized Exp.* **2010**, *45*, e2292; DOI: 10.3791/2292.
- [55] A. Ettenberg, H. O. Pettit, F. E. Bloom, G. F. Koob, *Psychopharmacology* **1982**, *78*, 204–209.
- [56] C. M. Olsen, D. S. Childs, G. D. Stanwood, D. G. Winder, *PLoS ONE* **2010**, *5*, e15085.
- [57] C. Chiamulera, M. P. Epping-Jordan, A. Zocchi, C. Marcon, C. Cottiny, S. Tacconi, M. Corsi, F. Orzi, F. Conquet, *Nat. Neurosci.* **2001**, *4*, 873–874.
- [58] C. W. Lindsley, B. S. Bates, U. N. Menon, S. Jadhav, A. S. Kane, C. K. Jones, A. L. Rodriguez, P. J. Conn, C. M. Olsen, D. G. Winder, *ACS Chem. Neurosci.* **2011**, *2*, 471–482.

Received: November 2, 2011

Published online on ■ ■ ■ ■, 0000

COMMUNICATIONS

R. Mueller, E. S. Dawson, J. Meiler,*
A. L. Rodriguez, B. A. Chauder, B. S. Bates,
A. S. Felts, J. P. Lamb, U. N. Menon,
S. B. Jadhav, A. S. Kane, C. K. Jones,
K. J. Gregory, C. M. Niswender, P. J. Conn,
C. M. Olsen, D. G. Winder, K. A. Emmitte,
C. W. Lindsley*



mGlu₅ IC₅₀ = 91 nM, 1.7% Glu Max

From ANNs to NAMs! Data from an experimental metabotropic glutamate receptor 5 (mGlu₅) high-throughput screen (HTS) were employed to train artificial neural networks (ANNs) based on 345 confirmed negative allosteric modulators (NAMs) and 155 774 inactive compounds. This effort identified two potent mGlu₅ NAMs with a unique chemotype. Optimization afforded a tool compound (shown), active in mouse models of anxiety and addiction.



Discovery of 2-(2-Benzoxazolyl amino)-4-Aryl-5-Cyanopyrimidine as Negative Allosteric Modulators (NAMs) of Metabotropic Glutamate Receptor 5 (mGlu₅): From an Artificial Neural Network Virtual Screen to an In Vivo Tool Compound